



Effects of heat treatment on the structural and electrical conductivity of $\text{Fe}_2\text{O}_3\text{-P}_2\text{O}_5\text{-PbO}$ glasses

Ahmed E. Hannora¹ · M. M. El-Desoky²

Received: 30 June 2019 / Accepted: 23 September 2019 / Published online: 26 September 2019
© Springer Science+Business Media, LLC, part of Springer Nature 2019

Abstract

Glasses having compositions $x\text{Fe}_2\text{O}_3\text{-(}80-x\text{)P}_2\text{O}_5\text{-}20\text{PbO}$ with $x=20, 25, 30, 35$ mol% were prepared by traditional glass melt-quenching method. The effects of the heat treatment of glasses on their structural and electrical conductivity were studied by X-ray diffraction (XRD), differential scanning calorimeter, density (ρ) and dc conductivity (σ). The glass transition temperature (T_g) was observed to increase with Fe_2O_3 content. The density of the prepared glass and corresponding glass-ceramics increases with Fe_2O_3 content. XRD of as-quenched glass samples confirm the amorphous nature. Triclinic lead iron phosphate $\text{PbFe}_2(\text{P}_2\text{O}_7)_2$ is the main crystalline ceramic phase formed after heat treatment at 973 K, of 20 and 25 Fe_2O_3 mol% with average crystallite size of 74 nm. Hexagonal iron phosphate FePO_4 phases appeared with Fe_2O_3 exceeded 30 mol%. The high-temperature conductivity is well explained by polaronic hopping conduction model. It is observed that in this system non-adiabatic hopping conduction is present. The longitudinal optical phonon frequency (ν_o) and density of state $N(E_F)$ of the prepared glass and corresponding glass-ceramics are reasonable for the localized states.

1 Introduction

Low softening temperature, low melt viscosity, high electrical conductivity and relatively high thermal expansion coefficients, makes phosphate glasses the object of deep scientific investigation and excellent candidates for industrial applications [1–4]. The heavy lead inclusion in phosphate glass matrix can be used as nuclear waste storage media and a scintillators for gamma-ray and neutron detection [5]. Polyphosphate chains neighboring are linked together by cross bonding between the metal cations (Pb) and the nonbridging oxygen atoms of each PO_4 tetrahedron [6–8]. The P–O–P bond between PO_4 tetrahedra is generally much stronger than the cross bonding between chains via the metal cation. But due to their poor mechanical properties and chemical durability its commercial application is limited [3]. Recently, the elastic properties of lead phosphate glasses were studied using an ultrasonic technique [9]. To improve

the stability of these glasses, it is necessity of incorporate cationic network modifiers, such as alkali, alkaline-earth and transition metals to creation of nonbridging oxygen in the matrix [10]. The addition of Fe_2O_3 enhance the poor chemical durability of phosphate and is more effective in stabilizing lead phosphate glasses more than other metal oxides [3, 7].

Transition metal oxide glasses display semiconducting properties due to the presence of transition metal particles in more than one valence state. In these materials the electrical conduction is due to the transport of electrons. The iron ions in iron phosphate glasses and corresponding glass-ceramics coexists in two different valence states, Fe^{3+} has a $3d^5$ electronic configuration and Fe^{2+} has a $3d^6$ electronic configuration with $S=5/2$ and 2, respectively [11–13]. Iron phosphate glasses are electronically conducting glasses with polaronic conduction mechanisms [14–16]. Conduction mechanism in alkali-free iron phosphate glasses is assumed to takes place by electrons migrating from low to high valence sites between Fe^{2+} and Fe^{3+} ions (hopping) usually termed small polaron hopping [17, 18]. Superior properties of glass-ceramics are useful for different technical wide range applications. Glass-ceramics transformation takes place by controlling the process of nucleation and crystallites growth [19, 20]. According to Musinu et al. [21], iron ion interacts with lead ions giving rise to a stable structural which could be responsible for

✉ Ahmed E. Hannora
Ahmed.Hannora@suezuniv.edu.eg

¹ Department of Science and Mathematical Engineering,
Faculty of Petroleum and Mining Engineering, Suez
University, Suez 43521, Egypt

² Department of Physics, Faculty of Science, Suez University,
Suez 43518, Egypt

the good chemical and mechanical properties of iron lead phosphate glasses. The average length of the polyphosphate chains decreases with the addition of iron oxide. The location of Fe^{3+} ions in the octahedral sites strength the cross-bonding between the polyphosphate chains which improve the durability of the glasses. The melting point of the glass former P_2O_5 is reduce by adding PbO while adding Fe_2O_3 improve the chemical resistance and to decrease the crystallization [22, 23]. Also, iron phosphates usually have a low melting temperature [24]. Iron ions act as both network former and modifier depending on the $\text{Fe}^{2+}/\text{Fe}^{3+}$ ratio, high content of Fe_2O_3 acts in the structure former [18, 25].

The aim of the present work is to prepare iron lead phosphate glasses and corresponding glass–ceramics with different Fe_2O_3 composition by replacing of P_2O_5 with Fe_2O_3 . The correlation between the structure and electrical properties have been examined. To investigate the structure and thermal stability of lead–iron phosphate glasses, X-ray diffraction (XRD) and differential scanning calorimetry (DSC) have been used. The dependence of the electrical conductivity upon temperature is discussed.

2 Experimental work

Four glass samples were prepared by melting reagent grade $\alpha\text{-Fe}_2\text{O}_3$ (99.9%, Alfa Aesar), P_2O_5 and PbO , (99.9%, Sigma-Aldrich). These samples have the molar formula $x\text{Fe}_2\text{O}_3-(80-x)\text{P}_2\text{O}_5-20\text{PbO}$ with $x=20, 25, 30, 35$ mol%. The glass systems were prepared by mixing specified weights of nominal composition and heated in a silica crucible at 1200°C for 15 min. The melt was then poured on a thick copper block and immediately quenched by pressing with another similar copper block to obtained bulk glass of about 2.0 mm in thickness.

XRD analysis was performed using a Siemens D5000 powder diffractometer equipped with Cu K α radiation (wavelength = 0.15406 nm) with a nickel filter at 40 kV and 30 mA. The diffractometer was operated within the range of $5 < 2\theta < 60$ degree using a step time of one second and a step size of 0.05. Thermal analysis was performed in the temperature range from room temperature to 853 K using differential scanning calorimetry NETZSCH DSC 204, with heating rate 10 K/min. The average density (ρ) of the glasses was measured at room temperature using Archimedes method with Toluene and Hexane as the immersion liquids. At least three samples of each glass were used to determine the density using the following relation;

$$\rho = \rho_L \left(\frac{W_a}{W_a - W_L} \right) \quad (1)$$

where W_a is the weight in air; W_L is the weight in liquid and ρ_L is the density of the liquid. The molar volume (V_m) was calculated from the formula;

$$V_m = \sum \frac{X_i M_i}{\rho} \quad (2)$$

where, X_i is the molar fraction of the oxide i and M_i is its relative molecular mass. Samples were grinded and polished with different grit sized emery paper to obtain parallel surfaces of thickness ranging between 1 and 1.3 mm. Silver paste electrodes deposited on both faces of the polished samples. A multimeter type Keithely 760 was used to collect the dc conductivity data. The dc conductivity of the present systems was measured at temperatures between room temperature and 423 K. The I–V characteristic between electrodes was confirmed.

3 Results and discussion

Figure 1 shows the XRD patterns obtained from the as-quenched glass samples with different Fe_2O_3 content. These patterns showed a characteristic broad hump without any sharp peaks which confirms the nature of present sample is pure amorphous and non-crystalline. Differential scanning calorimetry (DSC) technique was used to confirm glassy state and to study the thermal behavior of prepared glass samples. Figure 2 shows DSC curves of formed glasses with different Fe_2O_3 contents. Glass-transition temperature (T_g) at 748 K for 20% Fe_2O_3 sample followed by exothermic peak corresponds to the crystallization temperature (T_c) at 777 K. With increasing Fe_2O_3 content the T_g peak shifted to the higher temperature values up to 787 K for 35% Fe_2O_3 glass sample followed by exothermic peak (T_c) at 808 K. The

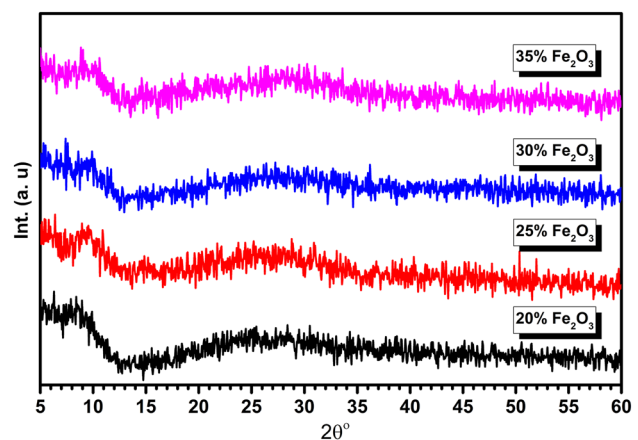


Fig. 1 XRD patterns of $x\text{Fe}_2\text{O}_3-(80-x)\text{P}_2\text{O}_5-20\text{PbO}$ glass samples for different Fe_2O_3 content

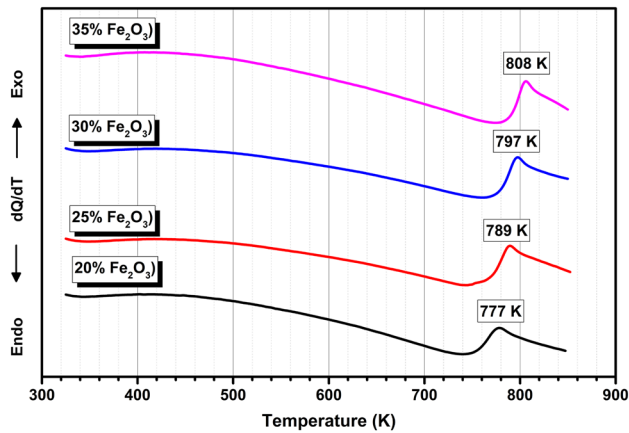


Fig. 2 DSC curve of $x\text{Fe}_2\text{O}_3-(80-x)\text{P}_2\text{O}_5-20\text{PbO}$ glass samples for different Fe_2O_3 content

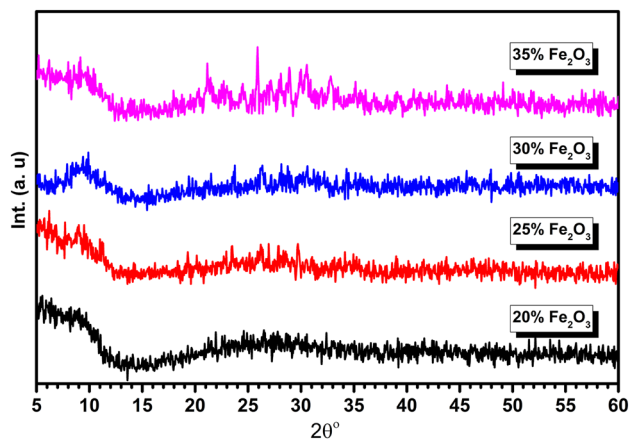


Fig. 3 XRD patterns of $x\text{Fe}_2\text{O}_3-(80-x)\text{P}_2\text{O}_5-20\text{PbO}$ glass samples for different Fe_2O_3 content after heat treatment at 873 K

larger the difference between the T_c and T_g is, the higher is the thermal stability of the glasses. As shown in Fig. 2, with increasing Fe_2O_3 content the thermal stability decreases.

Lead metaphosphate glass can be completely crystallized by heating the glass in air at 300 °C (573 K) for several hours, the addition of iron oxide to pure lead phosphate suppressed the evidence of crystallization [7]. $43\text{Fe}_2\text{O}_3-57\text{P}_2\text{O}_5$ and $10\text{ZnO}-30\text{Fe}_2\text{O}_3-60\text{P}_2\text{O}_5$ glasses have glass-transition temperature at ~ 790 K followed by the two exothermic peaks at ~ 910 and ~ 1070 K that are ascribed to the crystallization temperatures [11, 19].

After the heat treatment, the glasses were examined using X-ray diffraction powder diffractometer, Fig. 3. For all glasses, there was no evidence of crystallization or phase separation as a result of the heat treatment from 673 to 773 K for 2 h. Following the same heat treatment conditions at 873 K, X-ray analysis indicated that slight

crystallization and phase separation had occurred on the surface of the higher Fe_2O_3 content samples and phase/crystallinity increases with Fe_2O_3 content. According to Reis and Martinelli [22], Fe_2O_3 addition decrease the lead phosphate glasses crystallization. From Fig. 3, 20% Fe_2O_3 glass sample was the most stable sample with temperature, higher percentages show good tendency to glass crystallization. This XRD results confirms thermal stability by DSC. Lead–iron–phosphorus–oxygen network becomes stronger in compositions with an O/P ratio ~ 3.9 and (Fe + Pb)/P ratio ~ 0.90 [26].

Figure 4a shows XRD patterns of heat treated $25\text{Fe}_2\text{O}_3-55\text{P}_2\text{O}_5-20\text{PbO}$ glass samples at different temperatures for 2 h up to 973 K. Crystalline triclinic (or anorthic) lead iron phosphate single phase $\text{PbFe}_2(\text{P}_2\text{O}_7)_2$ (ICDD-JCPDS, No.: 01-087-1904) is formed after heat treatment. By using Rietveld refinement, the calculated lattice parameters of the formed triclinic phase were 0.4801 nm, 0.7088 nm, 0.7877 nm, 89.68°, 87.26° and 73.75°. As shown in Fig. 4a, the crystallinity increases with increasing heat treatment temperature. The lattice strain (ϵ) and crystallite sizes (D) can be estimated from the X-ray line broadening by using Williamson–Hall equation [27];

$$\beta \cos \theta = \frac{k\lambda}{D} + 4\epsilon \sin \theta \quad (3)$$

where β is the effective broadening, k is the shape factor (0.9), and λ is the wavelength of Cu- k_α radiation (0.15405 nm). Average crystallite size of ~ 74 nm and 0.4 lattice strain % were estimated from the plot of $\beta \cos \theta$ with respect to $4\sin \theta$. Figure 4b, shows XRD patterns of $35\text{Fe}_2\text{O}_3-45\text{P}_2\text{O}_5-20\text{PbO}$ glass samples at the same heat treatment conditions where crystalline monoclinic lead iron phosphate $\text{Pb}_3\text{Fe}_2(\text{PO}_4)_4$ (ICDD-JCPDS No.: 00-053-0175) and hexagonal iron phosphate FePO_4 (ICDD-JCPDS No.: 00-050-1635) are formed. The average crystallite size and strain % were 76 nm and 0.2, respectively.

Finally, from the XRD patterns of 25 mol% Fe_2O_3 , the only detected crystalline phase is the triclinic lead iron phosphate $\text{Fe}_2\text{Pb}(\text{P}_2\text{O}_7)_2$, with iron valence +3. The Fe^{2+} is present in residual amorphous phase [28]. This triclinic structure consists of $(\text{Fe}_3\text{O}_{12})^{16-}$ clusters, with Fe^{2+} ions in trigonal prism coordination are sandwiched between two Fe^{3+} ions in octahedral coordination which are connected by $(\text{P}_2\text{O}_7)^{4-}$ groups [26]. With higher Fe_2O_3 content, FePO_4 structure corresponds to ferric orthophosphate is formed. These results indicate that the origin of electrical conductivity of the present samples is due to small polaron hopping (SPH) between iron atoms of different valance states, i.e., a step-by-step electron hopping from Fe^{2+} to Fe^{3+} . According to [3, 18, 25], phosphate glass structure based on corner-sharing PO_4 tetrahedra. When Fe_2O_3 is added to a phosphate glass, the P–O–P bonds are replaced by P–O– Fe^{2+} and/or

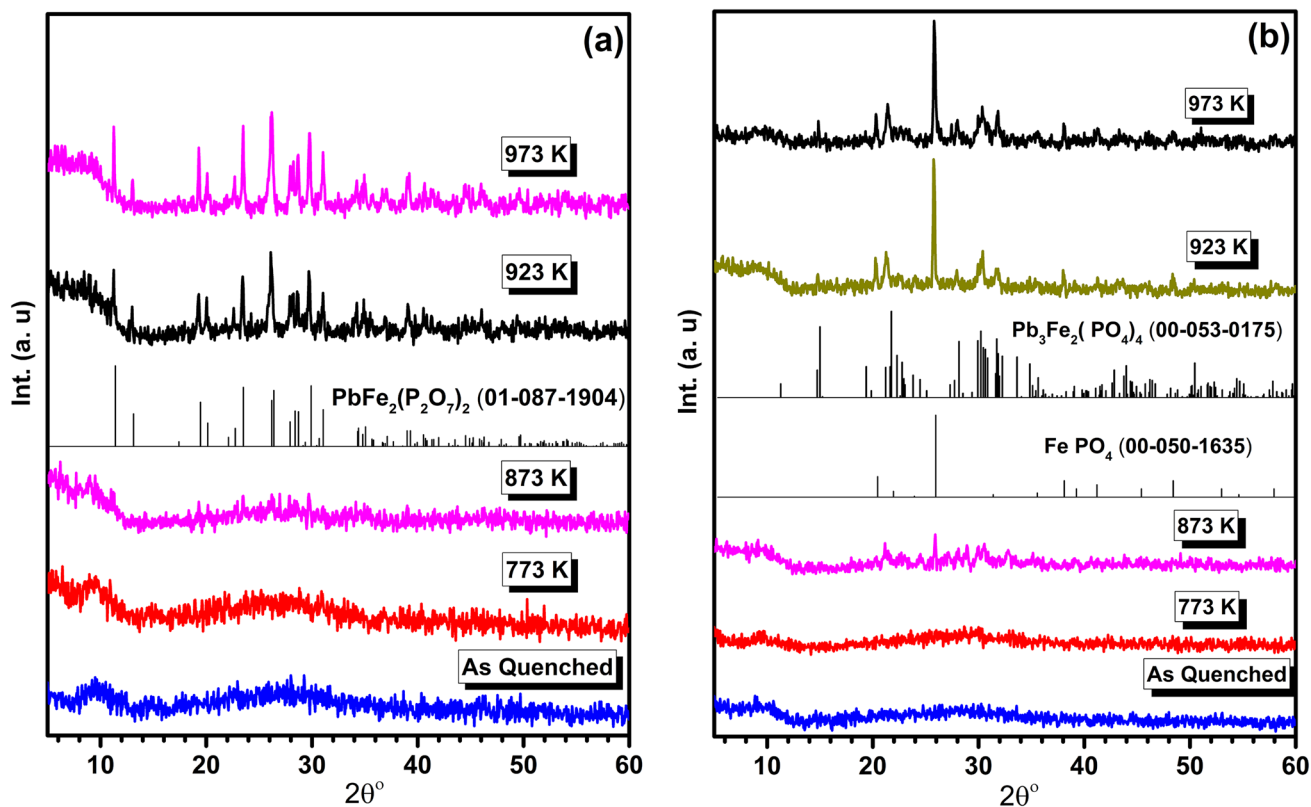


Fig. 4 XRD patterns of a $25\text{Fe}_2\text{O}_3\text{-}55\text{P}_2\text{O}_5\text{-}20\text{PbO}$ and b $35\text{Fe}_2\text{O}_3\text{-}45\text{P}_2\text{O}_5\text{-}20\text{PbO}$ glass samples after heat treatment at different temperatures

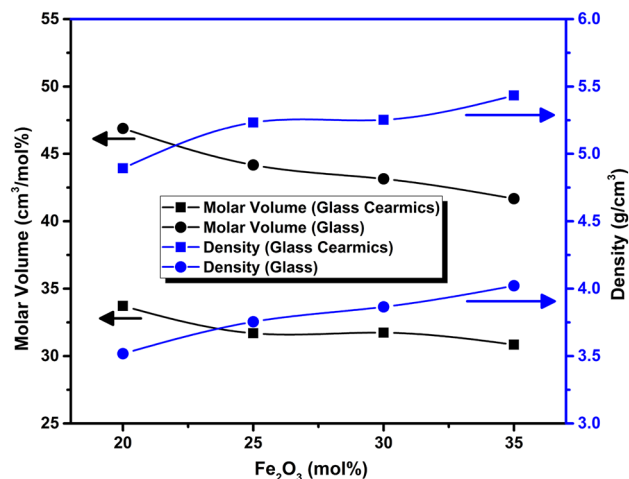


Fig. 5 Dependence of molar volume and density with Fe_2O_3 content of glasses and corresponding glass-ceramics

P–O– Fe^{3+} bonds where two valence state exists, as Fe^{2+} and Fe^{3+} and the $\text{Fe}^{2+} \rightleftharpoons \text{Fe}^{3+}$ equilibrium depends upon the melting conditions.

Figure 5 investigates the density and molar volume dependence on the Fe_2O_3 content in the glasses and corresponding glass-ceramics. In glass and glass-ceramics,

density gradually increases with increasing Fe_2O_3 content while molar volume shows opposite behavior. The molar volume of glass samples decreases from 46.88 to 41.68 cm^3/mol with increasing Fe_2O_3 . This could be due to the substitution of P by Fe atoms which makes the glass network structure denser. Glass-ceramics samples show the same trend, where the molar volume decreases from 33.71 to 30.84 cm^3/mol with increasing Fe_2O_3 . PbO up to 50 mol% enter the structure preferentially as network modifier forming non-bridging oxygen (NBO) ions ($\text{P}=\text{O}-\text{Pb}^{2+}\text{O}^-$) [29]. With increasing Fe_2O_3 content, the glasses and corresponding glass-ceramic structure becomes less open, allowing for the probable formation of decreasing number of nonbridging oxygen ions (NBOs). This may be due to the largest ionic radii and bond strength of Fe_2O_3 as compared to glass former P_2O_5 . As the Fe_2O_3 content increased the glass matrix becomes more compaction.

The logarithmic dc conductivity, σ , as function of reciprocal temperature of the present glasses and corresponding glass ceramics are shown in Fig. 6a, b. It is observed from the figure a linear temperature dependence up to a certain temperature ($\theta_D/2$, θ_D being the Debye temperature). Such behavior arises from the hopping of electrons or polarons between mixed valence states [4, 8, 18] as confirmed from XRD results. So the experimental conductivity data above

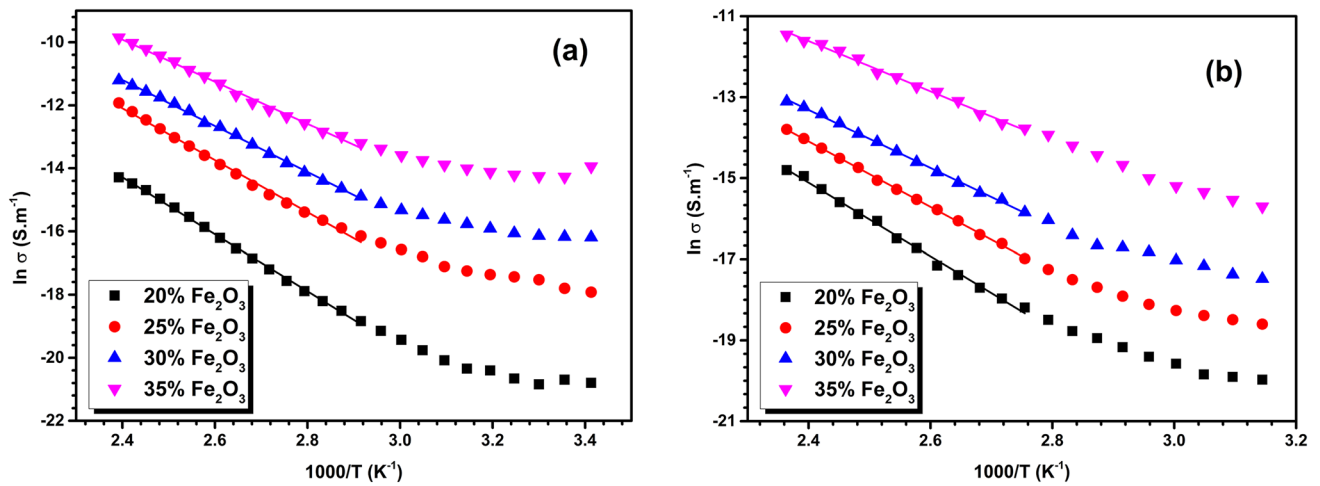


Fig. 6 Conductivity as a function of temperature for different Fe₂O₃ content of **a** glasses, **b** heat treated glasses (glass ceramics) at 600 °C/2 h

$\theta_D/2$ were fitted with the SPH model proposed by Austin and Mott [30, 31]. The high temperature activation energy was computed from the slope of each curve in the highest range of the temperature measured. The dc conductivity (σ) was calculated from;

$$\sigma = \frac{Id}{VA} \tag{4}$$

where I is the series current at temperature T , V is the applied dc voltage, d is the specimen thickness and A is the electrode area. The experimental conductivity data in such a situation is well described by activation energy for conduction given by Mott formula [31];

$$\sigma = \sigma_0 \exp\left(-\frac{W}{kT}\right) \tag{5}$$

and

$$\sigma_0 = \begin{cases} \nu_0 N e^2 R^2 C (1 - C) \exp(-2\alpha R) & \text{for non-adiabatic} \\ \nu_0 N e^2 R^2 C (1 - C) & \text{for adiabatic} \end{cases} \tag{6}$$

where σ_0 is the pre-exponent, W is the activation energy for the dc conductivity, k is the Boltzmann constant, T is the absolute temperature, R is interionic distance α , is the tunneling factor (the ratio of wave function decay), c the fraction of reduced transition metal ion.

The electrical conductivity of both glass and heat-treated glasses (glass-ceramics) increases with the increase of Fe₂O₃ content (Fig. 6a, b). A pronounced decrease in the electrical conductivity of the formed glasses is obtained after heat treatment at 873 K for 2 h, Fig. 6b. The activation energies were determined from the linear part of the high-temperature region of the plots, Fig. 6a, b, that follows

the Mott equation. The activation energy values for glass samples between 0.575 and 0.782 eV are very close to that of glass-ceramics (0.535 and 0.777 eV). Also, Fig. 6 shows that the natural logarithm of conductivity ($\ln \sigma$) at 373 K increases with Fe₂O₃ content while the activation energy (W) shows a reversed behavior in all glass and glass-ceramics samples. The addition of iron oxide to the phosphate network leads to breakdown of the P=O bonds and the P–O–P bonds are more chemically durable P–O–Fe²⁺ and/or P–O–Fe³⁺ bonds [3, 15]. The conductivity of glasses and corresponding glass-ceramics could be due the electron hopping from iron ions Fe⁺² and Fe⁺³.

Figure 7 presents conductivity variation with Fe₂O₃ content at a fixed temperature of glasses and corresponding glass-ceramics. It is interesting to note that glasses show high conductivity compared to glass ceramics. This can be

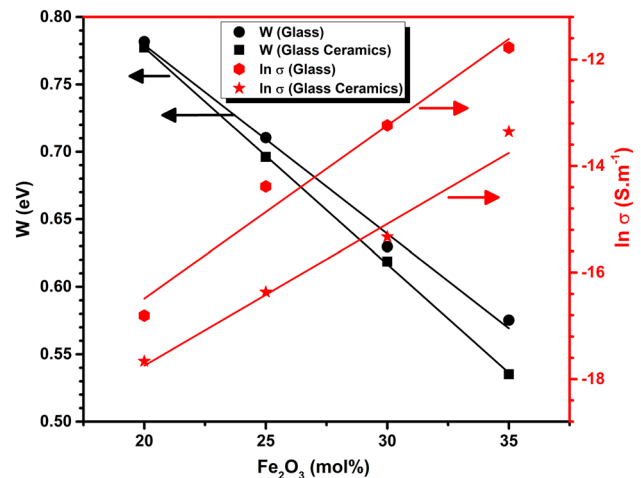


Fig. 7 Activation energy and conductivity dependence with Fe₂O₃ content of glasses and corresponding glass-ceramics

attributed to the improved crystallinity leading to reduction in the traps or size of the crystallites in the samples. The electrical conductivity is affected by grain boundary scattering. This grain boundaries act as traps which capture electrons and lead to the formation of a potential barrier. Building up of a negative charge and a potential barrier at the grain boundaries also causes scattering of conduction electrons, which decreases the conductivity. Based on the grain size effects of electrical conductivity, when the size of the crystalline grains is small, the grain boundary scattering increases significantly and can increase the conductivity. The electronic conductivity in lead iron phosphate glasses depends not only on the $\text{Fe}^{2+}/\text{Fe}_{\text{tot}}$ ratio, but also on the formation of the conduction pathways along and/or through the crystalline grains [32–34].

It is reported [33] that dc conductivity in iron phosphate glasses is electronic and strongly depends on the interionic distance (R) according to the relation;

$$R = \left(\frac{4\pi N}{3} \right)^{-\frac{1}{3}} \quad (7)$$

According to summarized values of R in Tables 1 and 2, R decreases with increasing Fe_2O_3 content. As R decreases it is reasonable to find an increase in dc conductivity.

The values of the polaron radii r_p calculated from [35];

$$r_p = \left(\frac{\pi}{6} \right)^{\frac{1}{3}} \frac{R}{2} \quad (8)$$

The density of states for thermally activated electron hopping near the Fermi level from basic principles is given as;

$$N(E_F) = \frac{3}{4\pi R^3 W} \quad (9)$$

The dc conductivity of these glasses is discussed on the basis of a polaron hopping conduction mechanism where the activation energy W is given by [30, 35].

$$W = \begin{cases} W_H + \frac{W_b}{2} & \text{for } T > \theta_D/2 \\ W_D & \text{for } T < \theta_D/4 \end{cases} \quad (10)$$

where W_H is the polaron hopping energy and is equal to $W_p/2$, W_p is the polaron binding energy and W_d is the disorder energy arising due to the energy difference of the neighboring sites at low temperature. θ_D is the Debye temperature and is defined by $h\nu_o = k\theta_D$, ν_o is the optical phonon frequency, h being Planck's constant and k is the Boltzmann constant. To determine ν_o for all different compositions, the Debye temperature θ_D was estimated by $T > \theta_D/2$ (Eq. 10). ν_o of the present glasses and corresponding glass ceramics where obtained to be in the range of 666–680 K and 703–711 K, respectively. The measured and calculated values of physical properties like content of iron ions (N), iron interionic distance (R), activation energy (W), polaron radii (r_p), Debye temperature (θ_D), longitudinal optical phonon frequency (ν_o) and density of state $N(E_F)$ of the prepared glass and glass–ceramics are summarized in Tables 1 and 2.

To explore the of hopping conduction nature (adiabatic or non-adiabatic), a plot of $\ln \sigma$ against activation energy W at a fixed experimental temperature (373 K) for glasses and corresponding glass–ceramics of different compositions has to be plotted, Fig. 8. This plot shows a straight-line nature, which indicate that the following dc conductivity equation is valid.

$$\sigma = c(1 - c) \frac{e^2}{RkT} \exp(-2\alpha R) \exp\left(-\frac{W}{kT}\right) = \sigma_o \exp\left(-\frac{W}{kT}\right) \quad (11)$$

From the slope, $1/kT$, if the value of the temperature is nearly equal to the observed temperature, then the hopping conduction is adiabatic in nature and it is mainly controlled by the activation energy. If the estimated and observed

Table 1 Physical parameters for different Fe_2O_3 content glass samples

Fe_2O_3 (mol%)	$N \times 10^{22}$ (cm^{-3})	R (nm)	W (eV)	r_p (nm)	ρ (g/cm^3)	θ_D (K)	$\nu_o \times 10^{13}$	$N(E_F) \times 10^{21}$
20	1.28	0.688	0.78	0.277	3.518	666	1.388	3.99
25	1.36	0.675	0.71	0.272	3.754	673	1.402	4.70
30	1.40	0.669	0.63	0.270	3.865	675	1.407	5.36
35	1.44	0.662	0.58	0.267	4.022	680	1.417	6.14

Table 2 Physical parameters for different Fe_2O_3 content glass–ceramics samples

Fe_2O_3 (mol%)	$N \times 10^{22}$ (cm^{-3})	R (nm)	W (eV)	r_p (nm)	ρ (g/cm^3)	θ_D (K)	$\nu_o \times 10^{13}$	$N(E_F) \times 10^{21}$
20	1.79	0.617	0.78	0.248	4.893	703	1.465	5.46
25	1.90	0.607	0.70	0.244	5.233	705	1.470	6.52
30	1.91	0.604	0.62	0.243	5.253	709	1.477	7.33
35	1.95	0.599	0.54	0.241	5.434	711	1.481	8.71

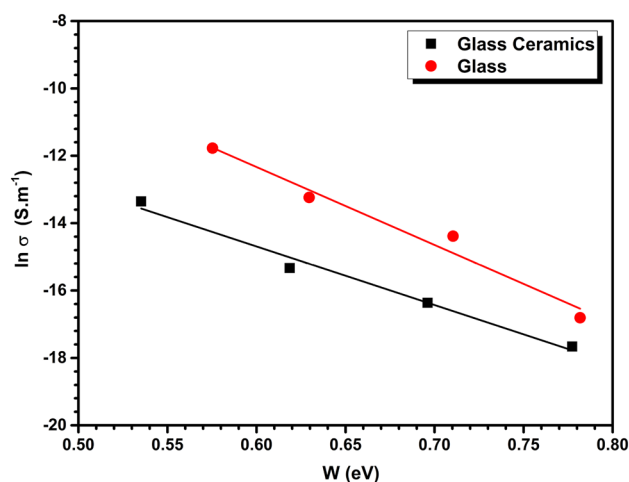


Fig. 8 Conductivity variation with activation energy at fixed temperature (373 K) of glasses and corresponding glass–ceramics

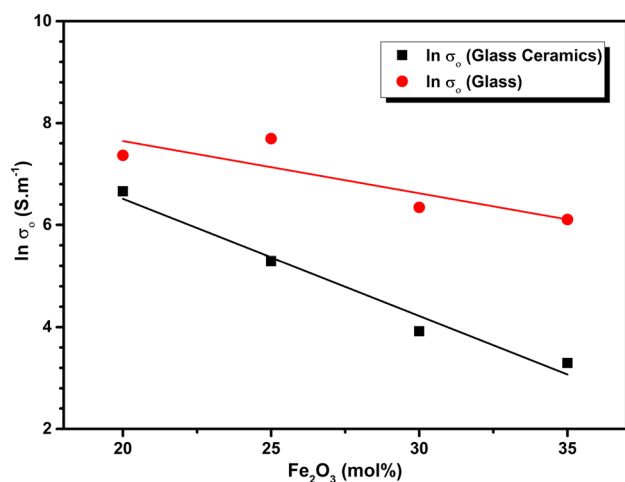


Fig. 9 Pre-exponential factor dependence with the Fe₂O₃ content of glasses and corresponding glass–ceramics

temperature values are very different; then this will suggest that the nature of the hopping conduction is non-adiabatic [36]. Figure 8 shows the relation between $\ln \sigma$ and activation energy W for glass and corresponding glass ceramics at fixed temperature (373 K). The estimated temperature calculated from the slope of the plot is differ than the experimental temperature (501 and 667 K) confirming that, the conduction mechanism in the present samples is due to non-adiabatic SPH of electrons [9]. Figure 9 presents the effect of Fe₂O₃ content on the pre-exponential factors (σ_0) obtained from the least squares straight line fits of the data σ_0 . The figure indicates a decrease in σ_0 with Fe₂O₃ content. From the above results, we conclude that again the conduction mechanism in the present samples is due to non-adiabatic hopping of the polarons.

From Tables 1 and 2, it can be observed that with increasing Fe₂O₃ content, the average interionic distance (R) decreases. Consequently, the addition of Fe₂O₃ leads to compaction of glass network which confirms density and molar volume results. The activation energy decreases with addition of Fe₂O₃. Also, as the average interionic distance (R) decrease, the activation energy decreases.

4 Conclusion

- From the XRD and DSC results all the samples were fully amorphous in nature, no crystalline phases were detected.
- The activation energy increases as the distance between iron ions, R , increases.
- In glasses and corresponding glass–ceramics, dc conductivity decreases with heat-treatment temperature.
- In glasses and corresponding glass–ceramics, the dc conductivity was found to increase as the iron content increases while the activation energy decreases.
- The glass transition temperatures were found to increase with the Fe₂O₃ content.
- The conduction is attributed to non-adiabatic hopping of small polaron (SPH).
- The parameters such as polaron radius and average separation between iron ions obtained from the fits of the experimental data to this model appear reasonable and are consistent with glasses and glass ceramics.

References

1. R.J. Amjad, M.R. Sahar, S.K. Ghoshal, M.R. Dousti, S. Riaz, B.A. Tahir, Optical investigation of Sm³⁺ doped zinc-lead-phosphate glass. *Chin. Phys. Lett.* **29**(8), 087304 (2012). <https://doi.org/10.1088/0256-307x/29/8/087304>
2. B.C. Sales, M.M. Abraham, J.B. Bates, L.A. Boatner, Structural properties of lead-iron phosphate glasses. *J. Non-Cryst. Solids* **71**(1), 103–112 (1985). [https://doi.org/10.1016/0022-3093\(85\)90279-0](https://doi.org/10.1016/0022-3093(85)90279-0)
3. A. Mogaš-Milanković, A. Šantić, L. Pavić, K. Sklepić, Iron phosphate glass-ceramics. *Croat. Chem. Acta* **88**(4), 553–560 (2015)
4. M.M. El-Desoky, F.A. Ibrahim, M.Y. Hassaan, Effect of sulfur addition on the transport properties of semiconducting iron phosphate glasses. *Solid State Sci.* **13**(8), 1616–1622 (2011). <https://doi.org/10.1016/j.solidstatesciences.2011.06.012>
5. C.C. Santos, I. Guedes, C.K. Loong, L.A. Boatner, A.L. Moura, M.T. de Araujo, C. Jacinto, M.V.D. Vermelho, Spectroscopic properties of Er³⁺-doped lead phosphate glasses for photonic application. *J. Phys. D* **43**(2), 025102 (2009). <https://doi.org/10.1088/0022-3727/43/2/025102>
6. Y.M. Lai, X.F. Liang, S.Y. Yang, J.X. Wang, B.T. Zhang, Raman spectra study of iron phosphate glasses with sodium sulfate. *J. Mol. Struct.* **1013**, 134–137 (2012). <https://doi.org/10.1016/j.molstruc.2012.01.025>

7. B.C. Sales, L.A. Boatner, Physical and chemical characteristics of lead-iron phosphate nuclear waste glasses. *J. Non-Cryst. Solids* **79**(1), 83–116 (1986). [https://doi.org/10.1016/0022-3093\(86\)90040-2](https://doi.org/10.1016/0022-3093(86)90040-2)
8. A. Al-Shahrani, A. Al-Hajry, M.M. El-Desoky, Electrical relaxation in mixed lithium and sodium iron phosphate glasses. *Physica B* **364**(1), 248–254 (2005). <https://doi.org/10.1016/j.physb.2005.04.016>
9. K.A. Matori, M.H.M. Zaid, S.H.A. Aziz, H.M. Kamari, Z.A. Wahab, Study of the elastic properties of $(\text{PbO})_x(\text{P}_2\text{O}_5)_{1-x}$ lead phosphate glass using an ultrasonic technique. *J. Non-Cryst. Solids* **361**, 78–81 (2013). <https://doi.org/10.1016/j.jnoncrsol.2012.10.022>
10. C.K. Loong, K. Suzuya, D.L. Price, B.C. Sales, L.A. Boatner, Structure and dynamics of phosphate glasses: from ultra- to orthophosphate composition. *Physica B* **241–243**, 890–896 (1997). [https://doi.org/10.1016/S0921-4526\(97\)00747-3](https://doi.org/10.1016/S0921-4526(97)00747-3)
11. L. Pavić, M.P.F. Graca, Ž. Skoko, A. Moguš-Milanković, M.A. Valente, Magnetic properties of iron phosphate glass and glass-ceramics. *J. Am. Ceram. Soc.* **97**(8), 2517–2524 (2014). <https://doi.org/10.1111/jace.12951>
12. A.V. Anupama, V. Kumaran, B. Sahoo, Application of mono-disperse Fe_3O_4 submicrospheres in magnetorheological fluids. *J. Ind. Eng. Chem.* **67**, 347–357 (2018). <https://doi.org/10.1016/j.jiec.2018.07.006>
13. A.V. Anupama, W. Keune, B. Sahoo, Thermally induced phase transformation in multi-phase iron oxide nanoparticles on vacuum annealing. *J. Magn. Magn. Mater.* **439**, 156–166 (2017). <https://doi.org/10.1016/j.jmmm.2017.04.094>
14. L. Pavić, Ž. Skoko, A. Gajović, D. Su, A. Moguš-Milanković, Electrical transport in iron phosphate glass-ceramics. *J. Non-Cryst. Solids* **502**, 44–53 (2018). <https://doi.org/10.1016/j.jnoncrsol.2018.02.012>
15. H. Doweidar, K. El-Egili, Y.M. Moustafa, I. Abbas, Density and dc conductivity of $\text{Fe}_2\text{O}_3\text{-PbO-P}_2\text{O}_5$ glasses. *Phys. Chem. Glasses: Eur. J. Glass Sci. Technol. B* **47**(5), 610–618 (2006)
16. H. Nasu, N. Soga, Temperature dependence of electrical conduction of sodium-iron phosphate glasses. *J. Non-Cryst. Solids* **53**(1), 123–134 (1982). [https://doi.org/10.1016/0022-3093\(82\)90022-9](https://doi.org/10.1016/0022-3093(82)90022-9)
17. A. Moguš-Milanković, B. Šantić, C.S. Ray, D.E. Day, Electrical relaxation in mixed alkali iron pyrophosphate glasses. *J. Non-Cryst. Solids* **263–264**, 299–304 (2000). [https://doi.org/10.1016/S0022-3093\(99\)00674-2](https://doi.org/10.1016/S0022-3093(99)00674-2)
18. A. Moguš-Milanković, D.E. Day, Thermally stimulated polarization and dc conduction in iron phosphate glasses. *J. Non-Cryst. Solids* **162**(3), 275–286 (1993). [https://doi.org/10.1016/0022-3093\(93\)91247-Z](https://doi.org/10.1016/0022-3093(93)91247-Z)
19. A. Moguš-Milanković, K. Sklepić, Ž. Skoko, L. Mikac, S. Musić, D.E. Day, Influence of nanocrystallization on the electronic conductivity of zinc iron phosphate glass. *J. Am. Ceram. Soc.* **95**(1), 303–311 (2012). <https://doi.org/10.1111/j.1551-2916.2011.04781.x>
20. M.M. El-Desoky, Giant electrical conductivity enhancement in $\text{BaO-V}_2\text{O}_5\text{-Bi}_2\text{O}_3$ glass by nanocrystallization. *Mater. Chem. Phys.* **119**(3), 389–394 (2010). <https://doi.org/10.1016/j.matchemphys.2009.09.011>
21. A. Musinu, G. Piccaluga, G. Pinna, Structural properties of lead-iron phosphate glasses by X-ray diffraction. *J. Non-Cryst. Solids* **122**(1), 52–58 (1990). [https://doi.org/10.1016/0022-3093\(90\)90224-A](https://doi.org/10.1016/0022-3093(90)90224-A)
22. S.T. Reis, J.R. Martinelli, Cs immobilization by sintered lead iron phosphate glasses. *J. Non-Cryst. Solids* **247**(1), 241–247 (1999). [https://doi.org/10.1016/S0022-3093\(99\)00078-2](https://doi.org/10.1016/S0022-3093(99)00078-2)
23. M.S. Al-Assiri, M.M. El-Desoky, Nanocrystallization as a method of improvement of electrical properties of $\text{Fe}_2\text{O}_3\text{-PbO}_2\text{-TeO}_2$ glasses. *J. Mater. Sci.: Mater. Electron.* **25**(9), 3703–3711 (2014). <https://doi.org/10.1007/s10854-014-2078-9>
24. A.P. Malakho, V.A. Morozov, K.V. Pokholok, B.I. Lazoryak, G. Van Tendeloo, Layered ordering of vacancies of lead iron phosphate $\text{Pb}_3\text{Fe}_2(\text{PO}_4)_4$. *Solid State Sci.* **7**(4), 397–404 (2005). <https://doi.org/10.1016/j.solidstatesciences.2005.01.007>
25. D.A. Magdas, O. Cozar, V. Chis, I. Ardelean, N. Vedeanu, The structural dual role of Fe_2O_3 in some lead-phosphate glasses. *Vib. Spectrosc.* **48**(2), 251–254 (2008). <https://doi.org/10.1016/j.vibspec.2008.02.016>
26. S.T. Reis, M. Karabulut, D.E. Day, Structural features and properties of lead-iron-phosphate nuclear wasteforms. *J. Nucl. Mater.* **304**(2), 87–95 (2002). [https://doi.org/10.1016/S0022-3115\(02\)00904-2](https://doi.org/10.1016/S0022-3115(02)00904-2)
27. V.D. Mote, Y. Purushotham, B.N. Dole, Williamson-Hall analysis in estimation of lattice strain in nanometer-sized ZnO particles. *J. Theor. Appl. Phys.* **6**(1), 6 (2012). <https://doi.org/10.1186/2251-7235-6-6>
28. S.T. Reis, D.L.A. Faria, J.R. Martinelli, W.M. Pontuschka, D.E. Day, C.S.M. Partiti, Structural features of lead iron phosphate glasses. *J. Non-Cryst. Solids* **304**(1), 188–194 (2002). [https://doi.org/10.1016/S0022-3093\(02\)01021-9](https://doi.org/10.1016/S0022-3093(02)01021-9)
29. H. Doweidar, Y.M. Moustafa, K. El-Egili, I. Abbas, Infrared spectra of $\text{Fe}_2\text{O}_3\text{-PbO-P}_2\text{O}_5$ glasses. *Vib. Spectrosc.* **37**(1), 91–96 (2005). <https://doi.org/10.1016/j.vibspec.2004.07.002>
30. I.G. Austin, N.F. Mott, Polarons in crystalline and non-crystalline materials. *Adv. Phys.* **18**(71), 41–102 (1969). <https://doi.org/10.1080/00018736900101267>
31. N.F. Mott, Conduction in glasses containing transition metal ions. *J. Non-Cryst. Solids* **1**, 1–17 (1968)
32. A. Šantić, Ž. Skoko, A. Gajović, S.T. Reis, D.E. Day, A. Moguš-Milanković, Physical properties of lead iron phosphate glasses containing Cr_2O_3 . *J. Non-Cryst. Solids* **357**(21), 3578–3584 (2011). <https://doi.org/10.1016/j.jnoncrsol.2011.07.011>
33. A. Moguš-Milanković, A. Šantić, A. Gajović, D.E. Day, Electrical properties of sodium phosphate glasses containing Al_2O_3 and/or Fe_2O_3 . Part II. *J. Non-Cryst. Solids* **296**(1), 57–64 (2001). [https://doi.org/10.1016/S0022-3093\(01\)00889-4](https://doi.org/10.1016/S0022-3093(01)00889-4)
34. M. Topić, A. Moguš-Milanković, D.E. Day, A study of polarization mechanisms in sodium iron phosphate glasses by partial thermally stimulated depolarization current. *J. Non-Cryst. Solids* **261**(1), 146–154 (2000). [https://doi.org/10.1016/S0022-3093\(99\)00601-8](https://doi.org/10.1016/S0022-3093(99)00601-8)
35. M.S. Al-Assiri, M.M. El-Desoky, Correlation between nanostructural and electrical properties of barium titanate-based glass-ceramic nano-composites. *J. Alloys Compd.* **509**(36), 8937–8943 (2011). <https://doi.org/10.1016/j.jallcom.2011.06.079>
36. M.M. El-Desoky, A. Al-Shahrani, Iron doping of semiconducting bismuth alkali borate glasses. *Physica B* **383**(2), 163–170 (2006). <https://doi.org/10.1016/j.physb.2006.01.518>

Publisher's Note Springer Nature remains neutral with regard to jurisdictional claims in published maps and institutional affiliations.